Increased Flooded Area and Exposure in the White Volta River Basin in Western Africa, Identified From Multi-source Remote Sensing Data

Chengxiu Li (✉ Chengxiu.Li@soton.ac.uk)
University of Southampton
Jadunandan Dash
University of Southampton
Moses Asamoah
University of Ghana
Justin Sheffield
University of Southampton
Mawuli Dzodzomenyo
University of Ghana
Solomon Hailu Gebrechorkos
University of Southampton
Daniela Anghileri
University of Southampton
Jim Wright
University of Southampton

Research Article

Keywords: disaster management, mapping system, NRT, SSA, satellite images, flood exposure

Posted Date: December 1st, 2021

DOI: https://doi.org/10.21203/rs.3.rs-1106820/v1

Version of Record: A version of this preprint was published at Scientific Reports on March 8th, 2022. See the published version at https://doi.org/10.1038/s41598-022-07720-4.

Abstract

Accurate information on flood extent and exposure is critical for disaster management in data-scarce, vulnerable regions, such as Sub-Saharan Africa (SSA). However, uncertainties in flood extent affect flood exposure estimates. This study developed a framework to examine the spatiotemporal pattern of floods and to assess flood exposure through utilization of satellite images, ground-based participatory mapping of flood extent, and socio-economic data. Drawing on a case study in the White Volta basin in Western Africa, our results showed that synergetic use of multi-temporal radar and optical satellite data improved flood mapping accuracy (77% overall agreement with participatory mapping outputs), in comparison with existing global flood datasets (43% overall agreement for the moderate-resolution imaging spectroradiometer (MODIS) Near Real-Time (NRT) Global Flood Product). Increases in flood extent were observed according to our classified product, as well as two existing global flood products. Flood exposure estimates remain highly uncertain and sensitive to the input dataset used, with the greatest farmland and infrastructure exposure estimated using a composite flood map derived from three products, with lower exposure estimated from each flood product individually. While population exposure varied greatly depending on the population dataset used. The study shows that there is considerable scope to develop an accurate flood mapping system in SSA and thereby improve flood exposure assessment and develop mitigation and intervention plans.

1. Introduction

Flood events occur frequently in many regions of SSA due to high climate variability and associated extreme precipitation events, with expectations that floods will become more frequent and extreme with climate change (Asare-Kyei et al. 2015). Growing population along with continued socio-economic changes such as urbanisation and farming expansion increase exposure to flooding (de Moel et al. 2011; Di Baldassarre et al. 2010; McGranahan et al. 2007) and may also exacerbate flood hazards. Flood exposure is predicted to double by 2050 in SSA (Jongman et al. 2012), resulting in large increases in flood risk (Afriyie et al. 2018; Hirabayashi et al. 2013; Winsemius et al. 2016). Flooding poses long-term challenges to livelihoods in SSA, not only through loss of lives, destruction of farmlands and infrastructure (Hirabayashi et al. 2013), but also disease outbreaks and worsened food and water security (Asare-Kyei et al. 2015).

The damaging impacts on livelihoods can be reduced by proper flooding mitigation strategies that are guided by sufficient flood hazard assessment, monitoring and early warning. However, lack of monitoring and information on flood extent and flood exposure hampers spatial targeting of effective mitigation strategies. Flood exposure, defined as population and assets located in flood-prone areas (Muis et al. 2015), however has received little attention to date (Smith et al. 2019). Assessing flood exposure of population and assets is particularly crucial in data scarcity region of SSA, particularly as it is the only global region showing increasing flood mortality rates since 1990 (Tanoue et al. 2016). Accuracte flood mapping and monitoring the location of people and assets exposure to flood can provide a foundation for flood risk assessment and mitigation that can help address the increase in mortality rates (Menoni et al. 2012).

The availability of accurate historical and current information on flood hazard events is particularly limited in SSA (UNDRR 2019). Flood hazard models have been implemented for flood forecasting and monitoring (Perera et al. 2019; Tarchiani et al. 2020). However, the accuracy of model-based flood hazard maps is restricted as it depends on the accuracy of various input data such as meteorological and topography data, thereby leading to greater uncertainty from error propagation (Ward et al. 2015). In addition, these flood hazard models tend to focus on the national or regional scale and are not designed for local-scale estimation where the impacts are experienced and local-level decision are required (Ward et al. 2015). Global scale flood datasets derived from satellite data are avaliable such as MODIS NRT Global Flood Product (Nigro et al. 2014) and the MODIS Global Flood Database (Tellman et al. 2021), The Global Flood Detection System (Kugler and De Groeve 2007). These datasets again have coarse-spatial resolution and validation of them is highly challenging, particulary in data-sparse regions such as SSA (Revilla-Romero et al. 2015) where accurate data is greatly needed for flood risk management. In this context, improving flood monitoring accuracy at local scale is greatly needed (Du et al. 2021; Singha et al. 2020).

Progresses have been made to provide flood monitoring at the local scale and over long term,

particularly with development in Earth Observation (EO) systems of increased revisit frequency and higher spatial resolution that are increasingly used in operational disaster monitoring systems (DeVries et al. 2020). Synthetic Aperture Radar (SAR) is particularly useful for flood mapping since it can provide frequent observations (Alsdorf et al. 2007; Ward et al. 2014) thanks to its capability to monitor land in almost any weather conditions (Cian et al. 2018; Marzano et al. 2012). Flooded areas generate a low backscatter signal and appear to be very dark in SAR images, which makes them distinguishable from other land cover classes such as agricultural land or built-up areas. Several SAR-based flood detection techniques have been proposed (Tsyganskaya et al. 2018), such as histogram thresholding or clustering (Martinis et al. 2009), change detection (Li et al. 2018; Long et al. 2014), and time series analysis (Cian et al. 2018). Defining a robust and objective threshold for classifying flooded area is one of the challenges in accurate flood mapping using the above methods (O'Grady et al. 2011). Currently, most studies are either based on a universal threshold value that may be unsuitable for specific sub-regions or dependent on user-defined empirical analysis, which makes it difficult to apply in different study regions. This study, however, propose an approach that define thresholds that tailed for local case study in an objective day, that is, through using optical satellite data to define thresholds for SAR-based flood mapping techniques. Optical satellite data have been also widely used for flood mapping and especially for long-term flood monitoring (Islam et al. 2010; Qi et al. 2009; Sheng et al. 2001), despite the impact of clouds during the rainy and flood season (Singha et al. 2020). Our study therefore use a combination of optical images and SAR images to improve existing algorithm for flood mapping using SAR data, as well as provide a more complete estimation of flood extent and enable long-term flood monitoring (Tong et al. 2018).

In addition, the lack of local ground data that used to evaluate the accuracy and limitations of satellite data-derived flood extent has been another major drawback in previous studies. Most studies that assess accuracy via inter-comparison of satellite-based flooding maps (DeVries et al. 2020; Singha et al. 2020), for example, optical satellite images which were used to evaluate the accuracy of flood mapping from radar satellite images (Singha et al. 2020), however often underestimate flood extent given high cloud occurrence

therefore providing insufficient accuracy assessment. This study instead collected ground data through participatory mapping to assess the accuracy of satellite-based flood maps. Participatory mapping, which engages local knowledge and expertise and allows local communities to delineate flood-affected extent on provided basemaps, has been widely recognized as an effective tool to collect and understand flood extent on the ground (Kienberger 2014). Involving communities' knowledge of floods through participatory mapping is critical in the data-scarce SSA context as communities experience flooding first hand. Despite the value of local experience and knowledge, very few attempts have been made to combine flood extent derived from satellite data and through participatory mapping (Asare-Kyei et al. 2015; de Andrade and Szlafsztein 2015; Xueliang et al. 2017) for evaluating satellite-derived flood extent accuracy. Such a comparison can not only enable accuracy assessment of satellite-derived flood extent, but also indicate flood-prone areas associated with high impacts for local communities.

This research, for the first time, employed a combination of top-down approaches based on multi-source EO measurements and a consultative approach via participatory mapping to map flooded areas and their dynamics. Further, it investigates the scale and severity of population, infrastructure and farmland exposure to flooding in the White Volta basin in Ghana. Specifically, this study aims to:

- Map flood area at fine spatial scale (i.e. 10 m) using multi-source satellite images (including Sentinel-1, Sentinel-2 and Landsat-8) and analyse flood area dynamics through comparison with existing global flood datasets (e.g. MODIS NRT Global Flood Product, The European Commission's Joint Research Centre (JRC) Global Flood Database, and JRC Global Surface Water dataset) over 2000-2020.
- Evaluate the accuracy of satellite-derived flood extent (from this study and the existing global flood datasets), through comparison with participatory mapping outputs.
- Estimate flood exposure by combining the satellite-derived flood datasets with socio-economic data including high-resolution population density (100 m and 30 m), land use (30 m) and key infrastructures.

2. Study Design And Study Area

This study is a component of wider programme that employed a mixed-methods monitoring flooding events and examining its impacts on livelihoods, healthcare utilisation, and water point quality (Li et al. 2021) in White Volta catchment in Western Africa. The study area White Volta catchment is located in Ghana (Fig. 1), a subbasin of the Volta river basin with most of the population relying on rain-fed agriculture (Antwi-Agyei et al. 2012). The region is prone to floods from torrential rainfall, potentially coupled with scheduled overspill from the Bagre Dam, Burkina Faso (Almoradie et al. 2020) with devastating effects on the livelihoods of the poor communities living in the basin. Flood risk affects particularly the North-eastern, Northern and Savannah regions of the White Volta Basin (Antwi-Agyei et al. 2012). Floods along the main course of the White Volta river have been a recurrent annual phenomenon from August to October in recent decade (Djimesah et al. 2018). Communities in northern Ghana are more vulnerable to flood hazards, with lower adaptive capacity and severer food insecurity than those in other parts of Ghana (Almoradie et al. 2020). The region, however, has seldom been studied to understand flood hazards and develop adaptation measures appropriate to local conditions (Almoradie et al. 2020). The current flood early warning system

operated by the National Disaster Management Organization (NADMO) has not been informed by comprehensive data on flood extent at high spatial resolution (Djimesah et al. 2018).

3. Data And Methods

3.1 Mapping the spatial and temporal distribution of flooding

We firstly mapped the monthly maximum flood extent at fine spatial scale (10 m) during the wet season (July-September) based on radar data from Sentinel-1 available from 2016 to 2020 and optical satellite data from Sentinel-2 and Landsat-8. Secondly, we assessed the spatiotemporal flood dynamics by combining outputs from this study with existing flood datasets (the JRC Global Surface Water dataset, MODIS NRT Global Flood product, and MODIS Global Flood Database). Thirdly, we collected ground data through participatory mapping to evaluate the accuracy of flood extent from the satellite data, and finally assess flood exposure through integration with land use, population and infrastructure map layers.

3.1.1 Flood mapping using Sentinel-1 data, Sentinel-2 and Landsat-8 data

We used the Sentinel-1 Synthetic Aperture Radar (SAR) C-band (5.4 GHz) data provided by the European Space Agency (ESA) (Torres et al. 2012). This global dataset has a 12 or 6 day revisit cycle depending on the availability of Sentinel-1B imagery (Malenovský et al. 2012) with a spatial resolution of 10 m. The level-1 Ground Range Detected (GRD) pre-processed product in Google Earth Engine was accessed and processed for the White Volta Basin, comprising 2148 scenes from 2016–2020. Only descending pathways were available in the study area and VV polarized data were used because of higher accuracy in detecting floods compared to VH, based on previous studies (Clement et al. 2018; Singha et al. 2020; Twele et al. 2016).

We examined the combination of three algorithms to map flooded areas, namely image thresholding method, the Change Detection and Thresholding (CDAT) and the Normalized Difference Flood Index (NDFI) algorithms. The flooded areas identified consistently from both the CDAT and NDFI detection algorithm was found to achieve higher flood mapping accuracy than alone (Singha et al. 2020). The CDAT algorithm uses multi-temporal SAR imagery and classifies flooded areas based on difference in backscatter between flood/post-flood and reference non-flooded images (Clement et al. 2018; Schlaffer et al. 2017). The NDFI also implements change detection principles, but combines a time series of images to compensate for changes in land cover and soil moisture, defined as in Equation (1) below (Cian et al. 2018). The image thresholding method was also examined in this study, as it is a straightforward approach based on a single image and setting pixels as flooded when the backscatter coefficient is lower than a certain threshold value (Mason et al. 2012; Schumann et al. 2010).

$$\text{E}\text{q}\text{u}\text{a}\text{t}\text{i}\text{o}\text{n} \left(1\right): \text{N}\text{D}\text{F}\text{I}= \frac{\text{m}\text{e}\text{a}\text{n} {\sigma }0\left(\text{"reference"}\right)-\text{m}\text{i}\text{n} {\sigma }0 ("\text{r}\text{e}\text{f}\text{e}\text{r}\text{e}\text{n}\text{c}\text{e}+\text{f}\text{l}\text{o}\text{o}\text{d}"$$

)}{\text{m}\text{e}\text{a}\text{n} {\sigma }0\left(\text{"reference"}\right)+\text{m}\text{i}\text{n} {\sigma }0("\text{r}\text{e}\text{f}\text{e}\text{r}\text{e}\text{n}\text{c}\text{e}+\text{f}\text{l}\text{o}\text{o}\text{d}")]}
Selecting non-flood reference images is key for change detection techniques (Hostache et al. 2012). We selected images in June given that this is a dry month with no flooding recorded in this area during 2016-2020 according to visual inspection of Sentinel-1 images. In addition, vegetation phenology in June is close to that in the flooding season starting from July, which minimizes the impact of seasonal variation in vegetation on backscattering. Mean value composites were generated for the reference month of June and a monthly minimal value composite image was generated for post-flood scenes to capture the maximum flood extent area.

Defining threshold values is another critical step for accurately mapping flood extent using the above three methods. For the change detection and NDFI methods, threshold values are normally determined by analysing a histogram of the distribution of backscatter difference or the NDFI index. The threshold criterion is defined based on various empirical analyses (Cian et al. 2018; Clement et al. 2018). Normally, the threshold criterion is used to classify flooding when the values are less than the mean pixel value minus the standard deviation of the entire image, times a coefficient of 1.5 (Cian et al. 2018; Clement et al. 2018). We examined the feasibility of this commonly-used threshold in our study area, as well as propose a new approach to objectively retrieve threshold fit to local case studies. We firstly introduced sub-basin boundaries, as our study area covers a relatively large spatial domain with heterogeneous land cover types. We then calculated the thresholds described above at sub-basin level for each month. In addition, to define a more objective threshold appropriate to this study, water bodies identified via optical satellite images Sentinel-2 and Landsat-8 indices, and the JRC Global Surface Water dataset (Pekel et al 2016) were used to define the thresholds for the Sentinel-1 images. Water bodies were classified using an algorithm with three widely used indices: Normalized Difference Vegetation Index (NDVI), Enhanced Vegetation Index (EVI) and the Modified Normalized Difference Water Index (mNDWI): *Water = (mNDWI > EVI or mNDWI > NDVI) and EVI < 0.1* (Wang et al. 2020). We calculated the percentile distributions of these indices for detected water bodies for each of the three flood detection methods (i.e. backscatter coefficient, backscatter coefficient difference between pre-flood and post-flood, and NDFI). For each index, the 95th percentile was used as a threshold. We also applied a median 3 × 3 pixel filter to remove speckle effects in SAR images for a smoother image (Singha et al. 2020). In addition, all clusters smaller than 10 pixels are excluded to reduce spurious flooded areas as the minimum mappable unit is clumps of approximately 10 pixels. Finally, any pixels falling on a slope of >5° via NASA's Shuttle Radar Topography Mission (SRTM) elevation dataset (Farr et al. 2007), where a flood would be unlikely, were excluded (Tellman et al. 2021). Flood mapping in urban areas, dense forest is challenging with Sentinel-1 data because of double-bounce effects, however as the White Volta basin is dominated by savanna and crop fields that were normally submerged under floods, and flooded forest and urban area is not extensive and so was not considered. All Sentinel-1 data acquisition and analysis were conducted in the Google Earth Engine platform (Gorelick et al., 2017).

3.1.2 Existing global flood datasets and CHIRPS precipitation data

Existing global satellite-derived flood datasets were compared with our Sentinel-1-derived flood extent data, firstly to evaluate their accuracy in flood detection in the White Volta basin, secondly to examine flood extent trends, and thirdly to generate a composite map based on the maximum flood extent from Sentinel-1 and global flood datasets. In addition, precipitation trends were analyzed to understand whether precipitation alone can explain the dynamics of changing flood extent. The global flood datasets are the JRC Global Surface Water dataset (Pekel et al 2016), and two datasets based on the moderate-resolution imaging spectroradiometer (MODIS) images: the MODIS NRT Global Flood Product (Nigro et al. 2014) and the MODIS Global Flood Database (Tellman et al. 2021). The MODIS-based datasets both used the band ratio water detection algorithms to map flood area (Nigro et al. 2014; Tellman et al. 2021). The MODIS NRT product is available daily from 2000-2020 at 250 m spatial resolution, however only data for 2016-2020 could be accessed for the White Volta basin. Since the MODIS Global Flood Database mainly maps large flood events documented by the Dartmouth Flood Observatory (DFO) from 2000 to 2018 (Tellman et al. 2021), this dataset is available on an event basis. In this study, monthly and yearly maximum flood extent were generated using the MODIS NRT product from 2016-2020, while yearly maximum flood extent was generated using the MODIS Global Flood Database from 2000-2018. The JRC Global Surface Water dataset was generated using Landsat 5, 7, and 8 satellite imagery from 2000-2019 at a higher spatial resolution of 30 m (Pekel et al 2016). It maps the location and temporal distribution of seasonal surface water over this 20-year period at monthly level, forming a proxy for monthly flood extent. Yearly maximum flood area was also calculated based on this dataset for a longer period (2000-2020). We compared monthly and yearly maximum flood extent derived from the above flood products with the Sentinel-1 flood extent from this study, and further estimated changes in flood extent over 2000-2020. The statistical significance of flood extent trends at basin level was assessed using the Mann–Kendall (MK) test (Yue and Wang 2002). The Climate Hazards Group InfraRed Precipitation with Station data (CHIRPS) dataset was used to examine the correlation between precipitation and flood extent. This dataset is a quasi-global rainfall dataset with spatial resolution of 0.05° covering over 30 years, derived from satellite imagery and combined with in-situ station data (Funk et al. 2015). Specifically, yearly daily maximum precipitation summed over the White Volta basin was calculated, and a linear regression was fitted to quantify the relationship between flood extent and precipitation.

3.1.3 Participatory mapping for accuracy evaluation

A participatory mapping campaign for flood map accuracy assessment was conducted in September 2020 during the flood period in Northern Ghana. Eight sites that have been the most flooding affected communities were selected based on stakeholder consultation from Disaster Management Organisation's (NADMO) district office during the pre-field survey period (Fig. 1). These sites were located in Talensi and Savelugu districts in the Upper Eastern Region and Northern regions of Ghana. Basemaps, generated from high-resolution Google satellite imagery with acquisition dates between 2016 and 2019, were provided to draw exact flood extent. Map scales varied between communities from 1:5,000 to 1:20,000, following recommended practice for participatory mapping (Forrester and Cinderby 2015). In total, 10 hardcopies of basemaps covering total area of 19 km^2 were used for participatory mapping, with more than one map covered for some sites. In each of the eight sites, the local assembly men/women were invited to draw the flooding extent. Assembly men/women are elected politicians familiar with the local environment and flood

situation through interaction with the populations they represent. They were firstly asked to identify key facilities such hospitals and schools on the hardcopy basemaps so that they could familiarize themselves with the map. They were then asked to delineate the extent of the maximum and the most recent flooded area they have experienced. The hardcopy basemaps were then scanned, georeferenced and digitized using the QGIS software (version 3.16.0). We then performed accuracy assessment through stratified sampling of flooded and non-flooded locations within the participatory mapping sites. A total of 200 sample points was collected for accuracy assessment, calculating the kappa coefficient, producer and user accuracy for our Sentinel-1 flood extent and global flood datasets separately. We published the flood extent data from participatory mapping (Moses Asamoah 2020), including digitalized flooded polygon, detailed field protocol and informed consent that was sought from all human subjects.

3.2 Flood exposure estimation

Spatial overlay between flood extent and map layers of population density, land use and key infrastructures were analyzed to estimate flood exposure. Two different gridded population density maps were used in this study: The High Resolution Settlement Layer (HRSL) and WorldPop dataset (Linard et al. 2012; Sorichetta et al. 2015). The HRSL dataset is based on identification of individual buildings from high-resolution satellite imagery and distribution of population census data among these buildings to produce population density maps at a spatial resolution of 30 m for the year 2015 (Tiecke et al. 2017). The WorldPop dataset is based on multi-variate random forest models that disaggregate areal head counts of census data at a spatial scale of 90 m. WorldPop Population layers from 2016-2020 were intersected with flood extent data for the same period, while fixed HRSL population data in 2015 were overlaid with flood maps. The spatial distribution of urban and agricultural land use was identified as follows (see Table 1). 1) The extent of land use of cities, towns, villages, farms and others were retrieved from OpenStreetMap, a global crowdsourced database of buildings and infrastructure (Haklay and Weber 2008). 2) Rural, semi-urban and urban land use areas were obtained from the Global Human Settlement Layer (GHSL), produced by JRC (Pesaresi et al. 2016). 3) Cropland and urban classes for 2020 were derived from the Globeland30 global land cover dataset, which has relatively good accuracy over Africa (Samasse et al. 2018; Wei et al. 2020). Similarly, the spatial distribution of key infrastructures was also used to map flood exposure including: 1) roads, dams, and water points obtained from OpenStreetMap; 2) potential geographic occupancy of domestic water points of boreholes and water wells, produced using a maximum entropy modelling technique combining observational water point data with environmental covariates to adjust for incomplete feature coverage (Yu et al. 2019); 3) health facilities of clinics and hospitals based on the dataset from the HealthSites initiative (https://healthsites.io/), though this dataset might not provide a comprehensive representation. To examine the impact of using different flood dataset on exposure assessment, flood maps derived from Sentinel-1 and existing global flood datasets were intersected with population, land use, and key infrastructure map layers separately. To preserve spatial heterogeneity, each dataset was resampled to match the finest spatial resolution dataset, namely the 10 m resolution of Sentinel-1.

Table 1
Socio-economic variables and datasets used for flood exposure analysis

Socio-economic variables	Dataset	Variable retrieved		Spatial resolution	Year	Reference
Population	High-Resolution Settlement Layer (HRSL)	Population density		30 m	2015	(Tiecke et al. 2017)
	WorldPop	Population density		90m	2020	(Linard et al. 2012; Sorichetta et al. 2015)
Land use	OpenStreetMap	Urban area	Building footprints, residential, cities, etc	-	-	Haklay and Weber 2008
		Rural area	Villages, towns			
		Farm	Farm			
	Global Human Settlement Layer (GHSL)	Rural, semi-urban, urban areas		-		(Pesaresi et al. 2016)
	Globeland30	Croplands, built-up area		30	2020	
Key infrastructures	OpenStreetMap	Roads, schools, hospitals,dams, parking, water wells, boreholes, etc		-	-	Haklay and Weber 2008
	HeathSites	Pharmacy, hospital, clinic		-	2020	https://healthsites.io/
	Domestic water points (Potential geographic occupancy)	Boreholes Water wells		1 km	2020	(Yu et al. 2019)

4. Results

4.1 Flood area delineation from multi-source satellite data

4.1.1 Flood mapping using Sentinel-1

When we implemented the NDFI and CDAT algorithms using histogram thresholds from previous studies based on empirical analysis (Clement et al. 2018; Long et al. 2014), we found that standalone

implementation of NDFI and CDAT algorithms estimate larger flood extent than combined algorithms, with a particularly high false detection rate for the NDFI algorithm (Fig. S1). Considering clear false detection of existing algorithm, this study therefore only demonstrated flood mapping outputs thereafter that based on the thresholds defined using optical satellite images. To define threshold, firstly the distribution Sentinel-1 backscatter coefficient, backscatter coefficient difference (pre-flood and post-flood) and NDFI within water bodies detected by optical satellite images were shown (Fig. 2). Largest water bodies and pixel counts were shown in September, followed by October and August in 2020. The backscatter coefficient of water bodies ranged from -13 to -30, and the backscatter coefficient difference between pre-flood and post-flood imagery ranged from -20 to 0.5, whilst the NDFI of water bodies ranged from 0.0625-0.5. Using 95th percentile as a threshold, a value of -15 for backscatter coefficient, -1.1 for backscatter coefficient difference and 0.14 for NDFI was identified as threshold for classifying flood extent using Sentinel-1 images (Fig. 2). When we apply these three thresholds corresponding to image thresholding, NDFI and CDAT algorithms, and identification of areas mapped by all three methods reduced flooding mapping uncertainty related to hilly topography (Fig. S1). Combining the image thresholding method with the CDAT and NDFI change detection algorithms particularly reduced false detection of flooding (Fig. S1). Therefore, only areas identified as flooded by all three methods were used in subsequent flood product comparisons, accuracy assessment and flood exposure assessment.

4.1.2 Comparison with MODIS and JRC datasets

When we mapped flood extent during the wet season from July to October (Fig. 1, Fig. 3) over 2016-2020 using Sentinel-1 imagery, flooding was absent in some months. When all data products were considered, the smallest flooded area observed in 2017 with inundation only in August, while largest area occurred in September 2020 (Fig. 3a). The timing of the most extended flood extent within year shifted from August-September in 2016-2018 to September-October in 2019 and 2020 (Fig. 3a). Sentinel-1 data with the highest resolution produced larger flood area estimates than MODIS NRT products for all but one month (September 2018) (Fig. 3a, Fig. 3b). The JRC Global Surface Water dataset estimated the smallest flooded area despite its finer spatial resolution (Fig. 3a). The MODIS Global Flood Database, however, only captured flood events in three years (2003, 2007, 2018) from the past 19 years (Fig. 3c). Combining advantages of each dataset, a composite of ourSentinel-1 based flood extent and existing global flood datasets estimated the largest flood area (totalling 3251 km^2 from 2016-2020) compared to each dataset separately, but still showed similar yearly variation (Fig. 3b). The different datasets all show a temporal trend of increasing flooded area over 2016-2020 (Fig. 3b). Over the longer-term period of 2000-2020, there is an increasing trend in flooded area (with an M-K test of P<0. 01), based on the JRC Global Surface Water dataset (Fig. 3c). This trend in flood extent could be explained partly by increasing precipitation, since precipitation alone explained 46.3% of variation of yearly flood extent from 2000-2020 (Fig. 3d).

4.1.3 Participatory mapping for accuracy assessment of satellite-derived flood extent

When local participants delineated the maximum and most recent flood extent, the most recent flooding extent was in September 2020 when the field campaign was taking place. This was also noted by participants to be the maximum flood extent that have experienced. Floods normally start to recede after 5-7 days according to participants. We found Sentinel-1-derived flood extent most closely matched the participatory mapping output, with an overall agreement of 0.77 (kappa=0.55), while the agreement was lower for the MODIS NRT flooding dataset (0.43, kappa: 0.16) and lowest for the Global Surface Water data (0.3, kappa:0.008) (Table.2). Flood extent from all datasets combined shows a marginal gain in accuracy (overall agreement: 0.78, kappa=0.57) in comparison to the participatory mapping (Table.2). When the participatory mapped flood extent was superimposed on those derived from satellite data, in all eight selected communities, local participants identified a larger flooded area extending beyond the area identified by each satellite-derived product (Fig. 2). Comparing the elevation of flooded areas identified by satellite data versus participatory mapping, the latter were on average 12 meters higher than those identified by satellite data (Fig. 4).

Table 2
Accuracy assessment of flood extent in September 2020 classified using Sentinel-1 imagery and via existing global flood datasets (MODIS NRT Global Flood Dataset and JRC (Landsat) Global Surface Water dataset) versus flooding delineated via participatory mapping

	Sentinel-1	MODIS NRT	Landsat	Composite
Overall Accuracy	0.77	0.43	0.3	0.78
Kappa	0.55	0.16	0.008	0.57
User Accuracy	0.57	0.36	0.3	0.58
Producer Accuracy	0.7	0.25	0.14	0.71

4.2 Flood exposure assessment

4.2.1 Population exposure

We estimated that around 32,555 - 87, 378 people (about 4.4-15.4% of the total population) have been exposed to at least one Sentinel-1 observed event since 2016, based on the WorldPop and HRSL datasets (Fig. 5). Since population exposure increases with flood area, the population exposure estimated from the MODIS NRT Global Flood Dataset was lower (19,920-52,246 people or 2.42%-9.6%) than that using Sentinel-1, whilst the greatest population exposure of around 42,272 - 117,717 people (5.46-20.8% of total population) was estimated using the composite flood maps (Fig. 5). Population exposure estimated using HRSL dataset is lower than that estimated using WorldPop, however the proportion of population is higher when using HRSL data. Although the population estimates vary markedly based on the population density dataset and flood dataset, the total population exposure increased over 2016-2020, with the highest population exposure in 2020 and the lowest is in 2017, corresponding to the highest and lowest flood extent respectively (Fig. 5).

4.2.2 Exposure of land use types and key infrastructure

Analysis of land use (urban, semi-urban and rural land use) and key infrastructure exposure for the largest flooding year 2020 showed that rural and farming areas are the most exposed to flooding, with 138.5 km^2 of rural area (7.12%) and 81.42 km^2 of farmland (1.05%). Hotspots of flood exposure of urban area (1.2 km^2, 0.06%) and key infrastructure such as schools and hospitals (0.06 km^2, 1.2%) were also detected, together with roads (75.6 km, 0.5%) and potential occupancy area of water points (169 km^2, 1.6%). Above estimations are based on flood extent from Sentinel-1 dataset, which were are lower than using the composite flood map, which provides the highest flood exposure (Fig. 6). Exposure estimates were the lowest using the MODIS flood dataset, and in particular, no infrastructure exposure was detected using this dataset (Fig. 6).

5. Discussion

Spatially detailed mapping of flood extent and exposure assessment is generally challenging for data-poor areas such as SSA. Efficient and pragmatic methods are critical for flood mapping and helping to mitigate flood impacts, but through validation of the available data is also necessary. This study, for the first time, combines participatory mapping and multi-source satellite data and socio-economic data to investigate flood extent dynamics and evaluate flood exposure in the White Volta basin in Ghana. Our results reveal both opportunities and challenges for monitoring floods using satellite data and suggests areas for further investigations. Our results further stress the need for implementing flood management strategies as we observed increasing flood hazards and exposures.

5.1.1 Accuracy of flood mapping using multi-source satellite data

Flood monitoring either from optical or radar satellite data has strengths and limitations. We proposed a transferable and objective approach for flood mapping combining both radar and optical satellite images, by applying a threshold identified from optical images and a combination of algorithms including CDAT, NDFI and image thresholding of radar images. Using Sentinel-1 SAR data, estimated flood area depended on the selected threshold values, which however is very sensitive to land cover and seasonal vegetation phenological variations, leading to differences in the SAR signals for the same inundated location at varying time periods through the season and from year to year (Singha et al. 2020). Most studies defined the threshold based on either empirical analysis or applying values from other studies' distributional analyses (Cian et al. 2018; Clement et al. 2018). This criterion is suitable when a large part of the study area is flooded. However, where flooding is limited, it tends to overestimate flood extent in a relatively large spatial domain with heterogeneous land cover types, such as for the White Volta basin (Fig. S1). Here we combined optical and radar satellite data and defined the threshold for Sentinel-1 images based on water bodies identified using Sentinel-2 and Landsat optical satellite data. We further demonstrated that flood mapping errors such as those introduced by radar shadow generated from the hilly terrain could be reduced by combining image thresholding with the CDAT and NDFI change detection algorithms (Fig. S1). Image

thresholding could minimize the effects of land cover changes when using change detection algorithms, while change detection algorithms detect additional floods and exclude permanent water bodies identified by image thresholding methods (Fig. S1).

Our study shows the potential of flood mapping using Sentinel-1 data, as well as the integration of multi-source satellite imagery and global flood datasets for greater accuracy in flood area estimation than when using a single optical satellite-based dataset (Table 2). Evaluating the accuracy of an existing global flood dataset, we found that the MODIS NRT Global Flood product shows lower overall accuracy (0.43) compared to flood extent derived using this study's Sentinel-1 based algorithm (0.77). The coarser spatial resolution of MODIS data generally captures large flood events but cannot detect small flooded areas especially when the area is lower than the pixel size of 250 m, therefore leading to a lower accuracy compared to Sentinel-1-derived flood mapping outputs. This shows the latter's advantages over other datasets with relatively high temporal and spatial resolution. The daily monitoring of the MODIS NRT dataset captures flood events more completely, and it is less impacted by clouds compared to the Global Surface Water dataset. The Global Surface Water dataset is not sufficient to assess specific flooding events due to its low accuracy (0.33) in delineating flooding, as it estimates the least area of flooding comparing with other datasets. The low accuracy might be related to cloud cover and coarse revisit time (16 days). However, this dataset could still provide insights into yearly variations and long-term dynamics. Our study showed that combining flood map layers from multiple sources including Sentinel-1-derived and existing flood datasets allows for more samples in time and therefore provides more complete monitoring of flood events, as a composite map showed a slight improvement in accuracy (0.78) (Fig. 4, Table 2). This further suggests that many global scale flood estimates using MODIS or Landsat images underestimate flood area and exposure. In particular, the MODIS Global Flood Database (Tellman et al. 2021) detected very few flood events in Northern Ghana. Similarly, flood exposure of population, farming area and water points using the global flood datasets might be underestimated. The implementation of existing global flood datasets and other satellite data (i.e. including Sentinel-1 data) is recommended for future flood mapping as it provide more complete flood and exposure assessment, with future potential of mapping near real time flooding at continental or even global scale (Matgen et al. 2020).

This study Integrate people's knowledge via participatory mapping for accuracy assessment of satellite-derived flood extent. By combining participatory mapping and satellite monitoring for flood mapping, our study indicates both strengths and limitations of satellite monitoring and participatory mapping. First of all, as a widely-used approach for environmental monitoring such as monitoring forest plantations (Koskinen et al. 2019) and degradation (Delgado-Aguilar et al. 2019), and ecosystem services (van Oort et al. 2015), participatory mapping has been proven as an effective tool for flood risk assessment (Kienberger 2014) and enhancing community resilience by integrating their knowledge on the causes and mitigation strategies of flooding. In this study, local key participants tend to delineate a larger flood extent with higher elevation than that detected via satellite imagery (Fig. 3). This indicates that Sentinel-1 data might not capture shallow inundated areas at higher elevation which however were identified by participants. This could further show that Sentinel-1 data might underestimate flood area, potentially because of the satellite's revisit frequency. Even though Sentinel-1 has a revisit period of 6 days, it could still underestimate flood area given that flooding receded within 5-7 days according to mapping participants. More frequent satellite observation is

critical for flood mapping, underlining the argument above for combining flood maps from both optical and radar satellite images with different revisit patterns, so as to compensate for the limitations of each data stream and provide a denser, more complete picture of flood events. On the other hand, the participatory mapping outputs cannot be considered as a definitive measure of flood extent given the uncertainties associated with respondent perception and recall. For example, studies have shown that communities with direct flood experience tend to overestimate danger (Renato et al. 2008; Wachinger et al. 2013). If such communities also over-estimate flood extent, this could account for greater flood coverage in the participatory mapping outputs compared to satellite-derived products. Indeed, we observed disagreements in drawing exact inundated boundaries between individuals during the field campaign, although final maps were created by selected key representatives best informed of their local environments and flood situations. Flooding could also have restricted participants' movements and thus limited their knowledge of its spatial extent despite participatory mapping taking place immediately after the flood season. Participatory mapping is inherently local in scope and carries limitations for accuracy assessment across a larger region.

5.1.2 Increasing flood exposure

Our study provided a comprehensive and a spatially detailed flood exposure assessment combining various socio-economic datasets. In the research literature, flood exposure assessment concerning the location of people and assets has rarely received attention (Smith et al. 2019). The few flood exposure assessment studies either mainly assess broad land cover classes such as 'urban area' (Ward et al. 2015) or only use population map layers (Smith et al. 2019). Understanding infrastructure exposure to flooding is also key for developing flooding mitigation strategies, but has received little attention. Taking advantage of global crowdsourced databases of buildings and infrastructure (i.e. OpenStreetMap) and recent updated land cover and population datasets, we found that flood exposure varied greatly depending on the flood extent and population density dataset used, which suggests that large uncertainties persist in flood exposure estimates, as also noted in the other study (Smith et al. 2019). The large difference in population exposure is related to the way populations are mapped. WorldPop data models non-zero population density across almost the entire region, showing that all flooded areas generate exposure (Fig. S2). While the HRSL dataset is based on classification building blocks from optical satellite data, thereby distributing populations across a smaller and concentrated area. This result has significant implications for end-users looking to use emerging flood risk data sets to inform decision-making and suggests uncertainties in existing studies. For example, studies might underestimate flood impacts such as on public heath when using the MODIS NRT flood dataset (Saulnier et al. 2018), since we found a lower flood area and lower level of flood exposure using MODIS data compared to using Sentinel-1 or a composite map. Moving forward, accurate, spatially detailed datasets representing flood extent as well as spatial heterogeneity of people and assets are clearly required. Otherwise, as demonstrated here, inaccurate representations of exposure may persist, rendering such estimates ineffective as a tool for decision-making. Nevertheless, we found that the number of people exposed to flooding increased from 2016 to 2020 irrespective of the population or flood dataset used. Increased population exposure mainly resulted from increasing flood extent, so similar increases in infrastructure and land use exposure would also be expected. Spatial information on all these types of flood

exposure is key for decision-makers looking to develop adaption and mitigation plans, particularly this information is lack in SSA.

6. Conclusions

Although there are several global flood monitoring programs delivering flood locations and flooded areas near real-time, these flood products are available at a coarse resolution and their accuracy in SSA is rather limited. Since increased flood events and increased flood mortality rates have been obsvered in SSA, further flood extents monitoring and exposure evaluation is merited. This study developed a framework for mapping flood extent and exposure using multi-source data in the White Volta basin in Ghana. Our results showed that the combined usage of optical and radar satellite data produced better flood mapping accuracy (77% overall agreement with participatory mapping outputs) than existing global flood product (i.e. 43% overall agreement for MODIS NRT Global Flood Dataset). Our results showed that existing global flood datasets (e.g. MODIS NRT Global Flood Product and MODIS Global Flood Database), however, underestimated flood extent, indicating there is a considerable scope to develop an accurate flood mapping system in SSA. Moving forward, we suggest that flood map layers from multiple sources (i.e. Sentinel-1-derived and existing flood datasets) should be combined for flood monitoring as it allows for more samples in time and therefore provides more complete monitoring of flood events.

We found flooding exposure assessments are sensitive to input datasets used, such as flood extent data and population layers. Despite inconsistency in input datasets, we found increased population exposure. We also targeted rural areas, farmland, and infrastructures where flood mitigation and adaptation should be prioritized. We observed that increased flood extent was closely related to greater precipitation in the White Volta region, therefore a robust framework for vulnerability and risk assessment is important to protect the rural communities from future flooding events. Our localized flood extent maps and flood exposure monitoring could help address this gap in flood forecasting and risk management in SSA.

Declarations

Data availability

Satellite imagery from Landsat-8 and Sentinel-2, Sentinel-1, the Global Surface Water dataset (Pekel et al 2016); The Shuttle Radar Topography Mission (SRTM, see Farr et al 2007) digital elevation data, WorldPop population dataset were accessed and processed through the Google Earth Engine platform (https://developers.google.com/earth-engine/datasets/catalog). OpenStreetMap road network data were accessed through https://download.geofabrik.de/africa.html. Catchment boundary data were accessed through the World WildLife Fund (WWF) HydroSHEDS web site https://www.hydrosheds.org/downloads. Health facilities data were accessed through HealthSite initiative https://healthsites.io/.The MODIS flood product is based on: NRT MODIS/Aqua+Terra Global Flood Product MCDWD_L3_NRT distributed from NASA LANCE. Available on-line [https://earthdata.nasa.gov/earth-observation-data/near-real-time/mcdwd-nrt]. DOI: 10.5067/MODIS/MCDWD_L3_NRT.061. The population dataset is accessed through www.worldpop.org. The High Resolution Settlement Layer (HRSL) is available at:

http://ciesin.columbia.edu/data/hrsl/#acknowledgements [Facebook Connectivity Lab and Center for International Earth Science Information Network - CIESIN - Columbia University. 2016. Source imagery for HRSL © 2016 DigitalGlobe. Accessed 25th June 2021]. The participatory mapping output generated in this study are available on https://doi.org/10.5258/SOTON/D1956.

In addition, ethical approval obtained from the Faculty of Environmental and Life Sciences ethical review committee, University of Southampton, UK (25/07/2020, Reference 54506.A2) and the Institutional Review Board of the Noguchi Memorial Institute for Medical Research, University of Ghana (04/03/2020, Reference NMIMR-IRB CPN 062/19-20).

Acknowledgements

This work was funded through the 'Building REsearch Capacity for sustainable water and food security In drylands of sub-saharan Africa' (BRECcIA) which is supported by UK Research and Innovation as part of the Global Challenges Research Fund, grant number NE/P021093/1.

Author contributions

CL, JW, and JD designed the study and developed the methodology. CL, MA, MD collected data. CL performed the analysis and drafted the first manuscript. JS, SG and DA reviewed and edited the manuscript. All authors contributed to the manuscript revision and agreed on the final manuscript.

Competing Interests Statement

The authors declare that they have no known competing financial interests or personal relationships that could have appeared to influence the work reported in this paper.

References

1. Afriyie, K., Ganle, J. K. & Santos, E. 'The floods came and we lost everything': weather extremes and households' asset vulnerability and adaptation in rural Ghana. *Climate and Development*, **10**, 259–274 (2018).
2. Almoradie, A. *et al.* Current flood risk management practices in Ghana: Gaps and opportunities for improving resilience. *Journal of Flood Risk Management*, **13**, e12664 (2020).
3. Alsdorf, D. E., Rodríguez, E. & Lettenmaier, D. P. (2007). Measuring surface water from space.*Reviews of Geophysics*, *45*
4. Antwi-Agyei, P., Fraser, E. D. G., Dougill, A. J., Stringer, L. C. & Simelton, E. Mapping the vulnerability of crop production to drought in Ghana using rainfall, yield and socioeconomic data. *Appl. Geogr*, **32**, 324–334 (2012).
5. Asare-Kyei, D., Forkuor, G. & Venus, V. Modeling Flood Hazard Zones at the Sub-District Level with the Rational Model Integrated with GIS and Remote Sensing Approaches., **7**, 3531–3564 (2015).
6. Cian, F., Marconcini, M. & Ceccato, P. Normalized Difference Flood Index for rapid flood mapping: Taking advantage of EO big data. *Remote Sensing of Environment*, **209**, 712–730 (2018).

7. Clement, M. A., Kilsby, C. G. & Moore, P. Multi-temporal synthetic aperture radar flood mapping using change detection. *Journal of Flood Risk Management*, **11**, 152–168 (2018).
8. de Andrade, M. M. N. & Szlafsztein, C. F. Community participation in flood mapping in the Amazon through interdisciplinary methods. *Nat. Hazards*, **78**, 1491–1500 (2015). de Moel, H., Aerts, J. C. J. H. & Koomen, E. Development of flood exposure in the Netherlands during the 20th and 21st century. *Glob. Environ. Change*, **21**, 620–627 (2011).
9. Delgado-Aguilar, M. J., Hinojosa, L. & Schmitt, C. B. Combining remote sensing techniques and participatory mapping to understand the relations between forest degradation and ecosystems services in a tropical rainforest. *Appl. Geogr*, **104**, 65–74 (2019).
10. DeVries, B. *et al.* Rapid and robust monitoring of flood events using Sentinel-1 and Landsat data on the Google Earth Engine. *Remote Sensing of Environment*, **240**, 111664 (2020).
11. Di Baldassarre, G. *et al.* (2010). Flood fatalities in Africa: From diagnosis to mitigation.*Geophysical Research Letters*, *37*
12. Djimesah, I. E., Okine, A. N. D. & Kissi Mireku, K. Influential factors in creating warning systems towards flood disaster management in Ghana: An analysis of 2007 Northern flood. *International Journal of Disaster Risk Reduction*, **28**, 318–326 (2018).
13. Du, J. *et al.* Satellite Flood Inundation Assessment and Forecast Using SMAP and Landsat. *IEEE Journal of Selected Topics in Applied Earth Observations and Remote Sensing*, **14**, 6707–6715 (2021).
14. Farr, T. G. *et al.* (2007). The Shuttle Radar Topography Mission.*Reviews of Geophysics*, *45*
15. Forrester, J. & Cinderby, S. *A Guide to using Community Mapping and Participatory-GIS* (Stockholm Environment Institute, University of York, In: York, 2015).
16. Funk, C. *et al.* The climate hazards infrared precipitation with stations—a new environmental record for monitoring extremes. *Scientific Data*, **2**, 150066 (2015).
17. Haklay, M. & Weber, P. OpenStreetMap: User-Generated Street Maps. *IEEE Pervasive Computing*, **7**, 12–18 (2008).
18. Hirabayashi, Y. *et al.* Global flood risk under climate change. *Nature Climate Change*, **3**, 816–821 (2013).
19. Hostache, R., Matgen, P. & Wagner, W. Change detection approaches for flood extent mapping: How to select the most adequate reference image from online archives? *International Journal of Applied Earth Observation and Geoinformation*, **19**, 205–213 (2012).
20. Islam, A. S., Bala, S. K. & Haque, M. A. Flood inundation map of Bangladesh using MODIS time-series images. *Journal of Flood Risk Management*, **3**, 210–222 (2010).
21. Jongman, B., Ward, P. J. & Aerts, J. C. J. H. Global exposure to river and coastal flooding: Long term trends and changes. *Glob. Environ. Change*, **22**, 823–835 (2012).
22. Kienberger, S. Participatory mapping of flood hazard risk in Munamicua, District of Búzi, Mozambique. *Journal of Maps*, **10**, 269–275 (2014).
23. Koskinen, J. *et al.* Participatory mapping of forest plantations with Open Foris and Google Earth Engine. *ISPRS Journal of Photogrammetry and Remote Sensing*, **148**, 63–74 (2019).

24. Kugler, Z. & De Groeve, T. *The Global Flood Detection System* (Office for Official Publications of the European Communities, In. Luxembourg, 2007).
25. Li, C. *et al. Growing spatial overlap between dam-related flooding, cropland and domestic water points: a water-energy-food nexus management challenge in Malawi and Ghana* (Frontiers in Water, 2021).
26. Li, S. *et al.* Automatic near real-time flood detection using Suomi-NPP/VIIRS data. *Remote Sensing of Environment*, **204**, 672–689 (2018).
27. Linard, C., Gilbert, M., Snow, R. W., Noor, A. M. & Tatem, A. J. Population Distribution, Settlement Patterns and Accessibility across Africa in 2010. *PLOS ONE*, **7**, e31743 (2012).
28. Long, S., Fatoyinbo, T. E. & Policelli, F. Flood extent mapping for Namibia using change detection and thresholding with SAR. *Environmental Research Letters*, **9**, 035002 (2014).
29. Malenovský, Z. *et al.* Sentinels for science: Potential of Sentinel-1, -2, and -3 missions for scientific observations of ocean, cryosphere, and land. *Remote Sensing of Environment*, **120**, 91–101 (2012).
30. Martinis, S., Twele, A. & Voigt, S. Towards operational near real-time flood detection using a split-based automatic thresholding procedure on high resolution TerraSAR-X data. *Nat. Hazards Earth Syst. Sci*, **9**, 303–314 (2009).
31. Marzano, F. S., Mori, S., Weinman, J. A. & Montopoli, M. Modeling Polarimetric Response of Spaceborne Synthetic Aperture Radar Due to Precipitating Clouds From X- to Ka-Band. *IEEE Transactions on Geoscience and Remote Sensing*, **50**, 687–703 (2012).
32. Mason, D. C., Schumann, G. J. P., Neal, J. C., Garcia-Pintado, J. & Bates, P. D. Automatic near real-time selection of flood water levels from high resolution Synthetic Aperture Radar images for assimilation into hydraulic models: A case study. *Remote Sensing of Environment*, **124**, 705–716 (2012).
33. Matgen, P. *et al.* (2020). Feasibility assessment of an automated, global, satellite-based flood-monitoring product for the Copernicus Emergency Management Service. EUR 30073 EN, Publications Office of the European Union, Luxembourg, ISBN 978-92-76-10254-0, doi:10.2760/653891, JRC119812, Ispra. In
34. McGranahan, G., Balk, D. & Anderson, B. The rising tide: assessing the risks of climate change and human settlements in low elevation coastal zones. *Environment and Urbanization*, **19**, 17–37 (2007).
35. Menoni, S., Molinari, D., Parker, D., Ballio, F. & Tapsell, S. Assessing multifaceted vulnerability and resilience in order to design risk-mitigation strategies. *Nat. Hazards*, **64**, 2057–2082 (2012).
36. Moses Asamoah, J. W., Li, C. & Opare-Boafo, M. S. Mawuli Dzodzomenyo (2020). Participatory flood extent in northern Ghana. In M. Asamoah (Ed.). UK:University of Southampton
37. Muis, S., Güneralp, B., Jongman, B., Aerts, J. C. J. H. & Ward, P. J. Flood risk and adaptation strategies under climate change and urban expansion: A probabilistic analysis using global data. *Science of The Total Environment*, **538**, 445–457 (2015).
38. Nigro, J., Slayback, D., Policelli, F. & Brakenridge, G. R. *NASA/ DFOMODIS Near Real-Time (NRT) Global Flood Mapping ProductEvaluation of Flood and Permanent Water Detection* (In: cience Systems and Applications, Inc, 2014).
39. NASA Goddard Space Flight Center

40. Dartmouth Flood Observatory,University of Colorado O'Grady, D., Leblanc, M. & Gillieson, D. Use of ENVISAT ASAR Global Monitoring Mode to complement optical data in the mapping of rapid broad-scale flooding in Pakistan. *Hydrol. Earth Syst. Sci*, **15**, 3475–3494 (2011).
41. Perera, D., Seidou, O. & Agnihotri, J. *Flood Early Warning Systems: A Review Of Benefits, Challenges And Prospects. UNU-INWEH Report Series, Issue 08* (United Nations University Institute for Water, Environment and Health, Hamilton, Canada. In, 2019).
42. Pesaresi, M. *et al.* p., & (2016). Operating procedure for the production of the Global Human Settlement Layer from Landsat data of the epochs 1975, 1990, 2000, and 2014. EUR 27741. Luxembourg (Luxembourg): Publications Office of the European Union. JRC97705. In
43. Qi, S. *et al.* Inundation Extent and Flood Frequency Mapping Using LANDSAT Imagery and Digital Elevation Models. *GIScience & Remote Sensing*, **46**, 101–127 (2009).
44. Renato, M., Igor, S. & Michele, S. Disaster preparedness and perception of flood risk: A study in an alpine valley in Italy. *Journal of Environmental Psychology*, **28**, 164–173 (2008).
45. Revilla-Romero, B. *et al.* On the Use of Global Flood Forecasts and Satellite-Derived Inundation Maps for Flood Monitoring in Data-Sparse Regions. *Remote Sensing*, **7**, 15702–15728 (2015).
46. Samasse, K., Hanan, N. P., Tappan, G. & Diallo, Y. Assessing Cropland Area in West Africa for Agricultural Yield Analysis. *Remote Sensing*, **10**, 1785 (2018).
47. Saulnier, D. D., Hanson, C., Ir, P., Mölsted Alvesson, H. & von Schreeb, J. The Effect of Seasonal Floods on Health: Analysis of Six Years of National Health Data and Flood Maps. *International journal of environmental research and public health*, **15**, 665 (2018).
48. Schlaffer, S., Chini, M., Giustarini, L. & Matgen, P. Probabilistic mapping of flood-induced backscatter changes in SAR time series. *International Journal of Applied Earth Observation and Geoinformation*, **56**, 77–87 (2017).
49. Schumann, G., Di Baldassarre, G., Alsdorf, D. & Bates, P. D. (2010). Near real-time flood wave approximation on large rivers from space: Application to the River Po, Italy.*Water Resources Research*,*46*
50. Sheng, Y., Gong, P. & Xiao, Q. Quantitative dynamic flood monitoring with NOAA AVHRR. *International Journal of Remote Sensing*, **22**, 1709–1724 (2001).
51. Singha, M. *et al.* Identifying floods and flood-affected paddy rice fields in Bangladesh based on Sentinel-1 imagery and Google Earth Engine. *ISPRS Journal of Photogrammetry and Remote Sensing*, **166**, 278–293 (2020).
52. Smith, A. *et al.* New estimates of flood exposure in developing countries using high-resolution population data. *Nat. Commun*, **10**, 1814 (2019).
53. Sorichetta, A. *et al.* High-resolution gridded population datasets for Latin America and the Caribbean in 2010, 2015, and 2020. *Scientific Data*, **2**, 150045 (2015).
54. Tanoue, M., Hirabayashi, Y. & Ikeuchi, H. Global-scale river flood vulnerability in the last 50 years. *Sci. Rep*, **6**, 36021 (2016).

55. Tarchiani, V. *et al.* Community and Impact Based Early Warning System for Flood Risk Preparedness: The Experience of the Sirba River in Niger. *Sustainability*, **12**, 1802 (2020).
56. Tellman, B. *et al.* Satellite imaging reveals increased proportion of population exposed to floods., **596**, 80–86 (2021).
57. Tiecke, T. *et al.* (2017). Mapping the world population one building at a time. *ArXiv, abs/1712.05839*
58. Tong, X. *et al.* An approach for flood monitoring by the combined use of Landsat 8 optical imagery and COSMO-SkyMed radar imagery. *ISPRS Journal of Photogrammetry and Remote Sensing*, **136**, 144–153 (2018).
59. Torres, R. *et al.* GMES Sentinel-1 mission. *Remote Sensing of Environment*, **120**, 9–24 (2012).
60. Tsyganskaya, V., Martinis, S., Marzahn, P. & Ludwig, R. SAR-based detection of flooded vegetation – a review of characteristics and approaches. *International Journal of Remote Sensing*, **39**, 2255–2293 (2018).
61. Twele, A., Cao, W., Plank, S. & Martinis, S. Sentinel-1-based flood mapping: a fully automated processing chain. *International Journal of Remote Sensing*, **37**, 2990–3004 (2016).
62. UNDRR, C. (2019).Ghana Disaster Risk Profile
63. van Oort, B. *et al.* Assessing community values to support mapping of ecosystem services in the Koshi river basin, Nepal. *Ecosystem Services*, **13**, 70–80 (2015).
64. Wachinger, G., Renn, O., Begg, C. & Kuhlicke, C. The Risk Perception Paradox—Implications for Governance and Communication of Natural Hazards. *Risk Anal*, **33**, 1049–1065 (2013).
65. Wang, X. *et al.* Gainers and losers of surface and terrestrial water resources in China during 1989–2016. *Nat. Commun*, **11**, 3471 (2020).
66. Ward, D. P. *et al.* Floodplain inundation and vegetation dynamics in the Alligator Rivers region (Kakadu) of northern Australia assessed using optical and radar remote sensing. *Remote Sensing of Environment*, **147**, 43–55 (2014).
67. Ward, P. J. *et al.* Usefulness and limitations of global flood risk models. *Nature Climate Change*, **5**, 712–715 (2015).
68. Wei, Y., Lu, M., Wu, W. & Ru, Y. Multiple factors influence the consistency of cropland datasets in Africa. *International Journal of Applied Earth Observation and Geoinformation*, **89**, 102087 (2020).
69. Winsemius, H. C. *et al.* Global drivers of future river flood risk. *Nature Climate Change*, **6**, 381–385 (2016).
70. Xueliang, C., Tamiru, A., James, H., Everisto, M., Luxon, N. & M., & Living with floods – Household perception and satellite observations in the Barotse floodplain, Zambia. *Physics and Chemistry of the Earth, Parts A/B/C*, **100**, 278–286 (2017).
71. Yu, W. Y. *et al.* (2019). Mapping access to domestic water supplies from incomplete data in developing countries: An illustrative assessment for Kenya. *Plos One, 14*
72. Yue, S. & Wang, C. Y. Applicability of prewhitening to eliminate the influence of serial correlation on the Mann-Kendall test. *Water Resour. Res*, **38**, 4–1 (2002). -4-7

Figures

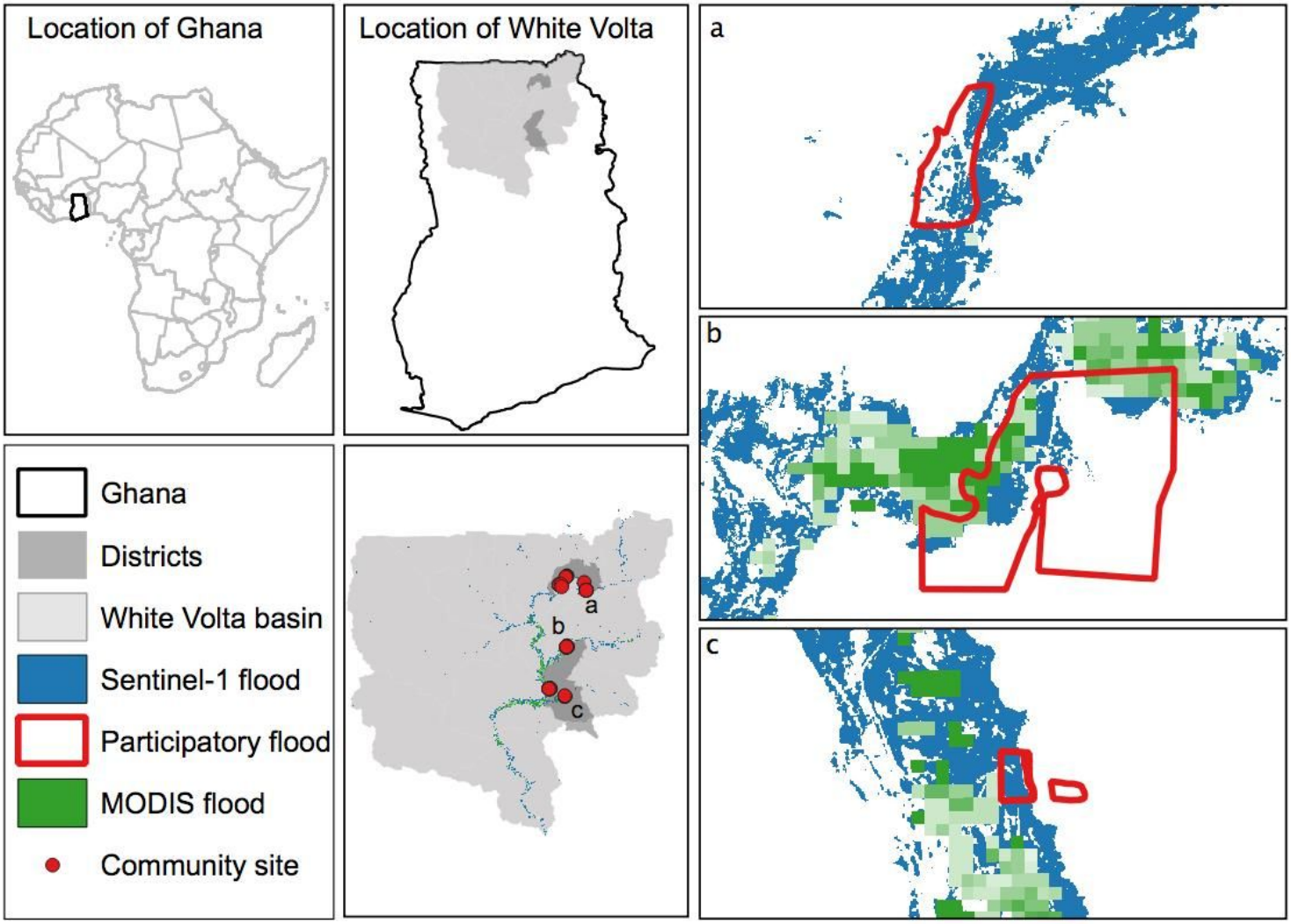

Figure 1

Location of study area and flood area retrieved using Sentinel-1 data (blue) for 2020 and most recent flood area identified by local participants (red boundary) using participatory mapping

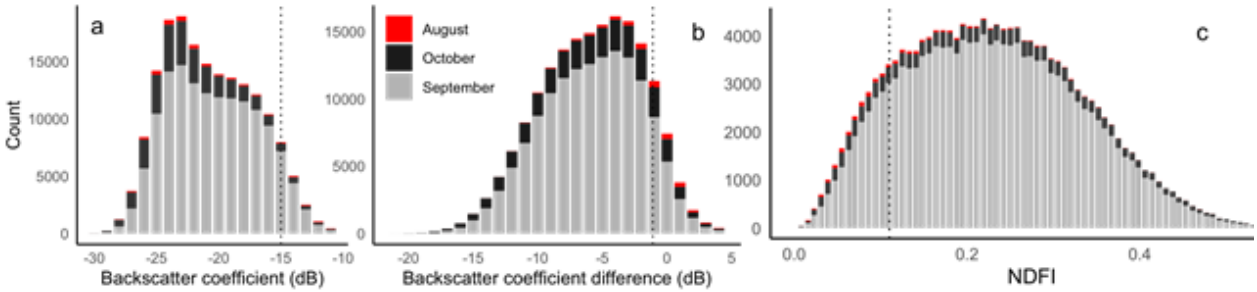

Figure 2

Histograms showing the distribution of backscatter coefficient (left) of water bodies, backscatter coefficient difference (middle), and NDFI (right) between pre-flood (June) and post-flood periods identified by a water

detection algorithm (NDWI) using optical satellite data (Sentinel-2 and Landsat-8) for August, September and October 2020. Dashed line indicates 95th percentile of backscatter coefficient distribution, 5% percentile of NDFI distribution.

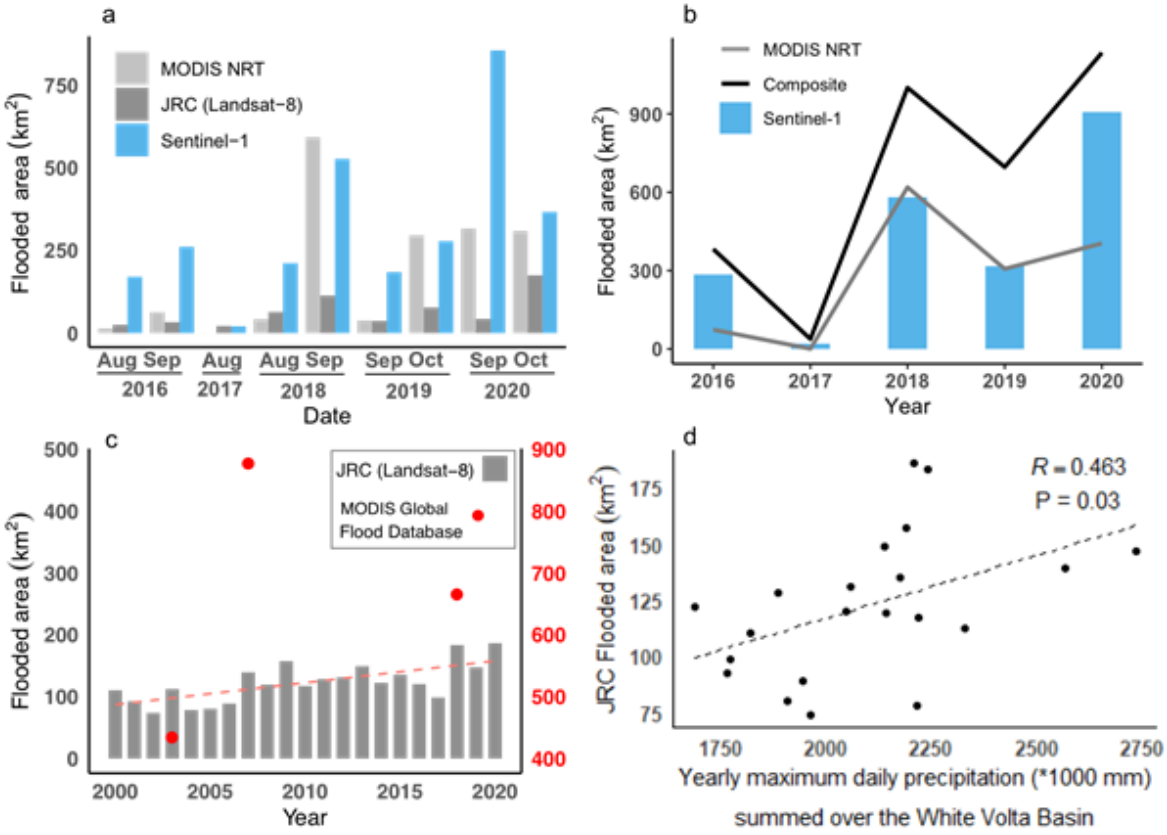

Figure 3

Comparison of flooded area estimated using Sentinel-1 from this study and existing global flood datasets (MODIS NRT Global Flood Dataset, MODIS Global Flood Database, JRC Global Surface Water dataset). a) Maximum flood area for wet season from 2016-2020. b) Yearly maximum flood area comparison between MODIS NRT datasets, Sentinel-1 and composite flood dataset from 2016-2020 c) Flood area dynamics based on the JRC Global Surface Water dataset from 2000-2020 and MODIS Global Flood Database. d) Correlation between flooding area based on JRC datasets and yearly precipitation.

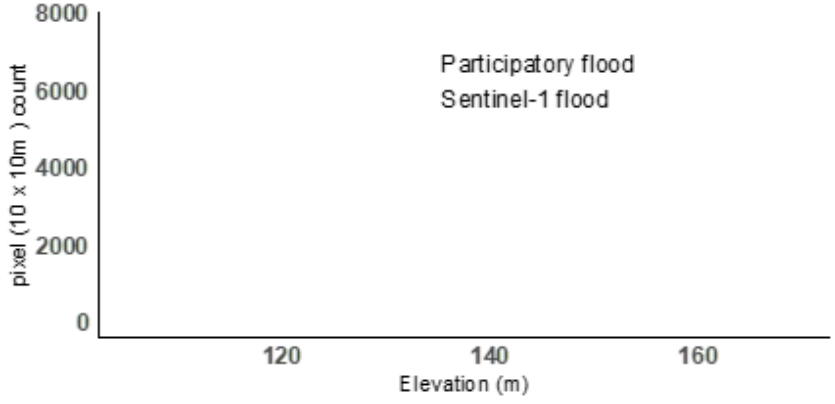

Figure 4

Elevation difference between flood area identified by local key participants using participatory mapping and Sentinel-1 satellite data

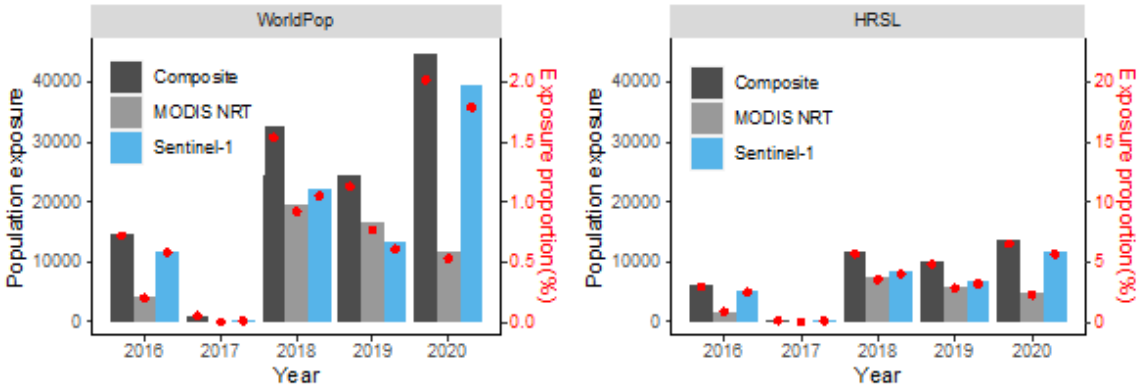

Figure 5

Total and proportion of population exposed to flooding from 2016-2020 estimated through spatial overlay of two population datasets (WorldPop, HRSL) with flood datasets

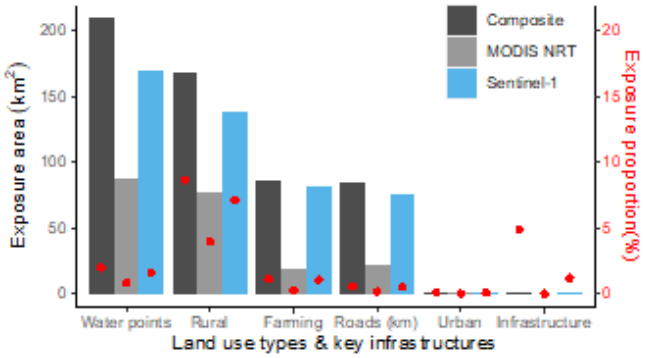

Figure 6

Land use areas and key infrastructures exposed to flooding in 2020

Supplementary Files

This is a list of supplementary files associated with this preprint. Click to download.

- SuppleFloodMappingWhiteVoltaFinal.docx